Influence of crystal chemistry on ideal plastic shear anisotropy in forsterite: First principle calculations

Julien Durinck, A. Legris, Patrick Cordier

American Mineralogist, Volume 90, pages 1072–1077, 2005

Influence of crystal chemistry on ideal plastic shear anisotropy in forsterite: First principle calculations

JULIEN DURINCK,[1] ALEXANDRE LEGRIS,[2] AND PATRICK CORDIER[1,*]

[1]Laboratoire de Structure et Propriétés de l'Etat Solide, UMR CNRS 8008, Université des Sciences et Technologies de Lille, 59655 Villeneuve d'Ascq Cedex, France
[2]Laboratoire de Métallurgie Physique et Génie des Matériaux, UMR CNRS 8517, Université des Sciences et Technologies de Lille, 59655 Villeneuve d'Ascq Cedex, France

ABSTRACT

We present ab initio calculations of ideal shear strengths (ISS) in forsterite at zero temperature using pseudopotential density functional theory within the generalized gradient approximation. A localized rigid-body shear is imposed on a given plane of an infinite defect-free crystal. The energy increase associated with this shear (called the generalized stacking fault energy) gives access to the ISS. The goal of this study is to assess the influence of crystal chemistry on the intrinsic resistance of plastic shear of a mineral like forsterite. ISS have been calculated for plastic shear along [100], [010], and [001] in various potential glide planes of forsterite. We show that the [001] slip, which corresponds experimentally to an easy glide at low temperature, exhibits the lowest energy barrier. The [010] glide is precluded because it involves very unfavorable atom impingements.

INTRODUCTION

The mechanical properties of olivine have been of long-standing interest as this mineral dominates the Earth's upper mantle. This layer extends down to the transition zone (starting at ca. 410 km depth) where olivine transforms into its high-pressure polymorphs. The upper mantle is an important boundary layer, not only because it represents about 20% of the volume of the Earth, but also because flow in the asthenospheric mantle is largely responsible for driving plate tectonics.

Reflecting this strong interest, a large body of experimental deformation data [mostly at room or low (300 MPa) pressure, see below] are available that address the mechanical properties of olivine. Except shock experiments, which represent a special case, most experiments have focused on the high-temperature (i.e., above ca. 1000 °C) mechanical properties, emphasizing the complex influence of point defect chemistry (including water-related defects) on olivine plastic behavior. The recent development of high-pressure deformation experiments raises the question of the influence of pressure on plastic deformation of minerals and challenges our understanding of their deformation mechanisms. On the theoretical side, however, not many studies have been devoted to the fundamentals of plastic deformation of olivine. The recent rapid developments of large-scale computing capabilities now allow us to address mechanical properties from a fundamental perspective. In materials with simple structures, like metals, it is now possible to model dislocation cores, and also fundamental processes like cross-slip, using atomic-scale simulations relying on empirical potentials (Rasmussen et al. 1997). In mineral physics, this approach is not yet very developed. One of the advantages of ab initio calculations is that the chemical complexity (for which an empirical potential description is either not available or not reliable) does not have to be taken into account explicitly, the interaction between the atoms being fully described by a universal functional of the electronic density (see below). This allows us to address complex systems such as minerals with relatively low symmetries and large unit cells containing several kinds of atoms. Indeed, it is likely that such complex crystal chemistry has profound implications on plastic properties. From a fundamental point of view, plastic shear has to localize on specific planes which, in silicate minerals, are often located on cationic layers between the SiO_4 tetrahedra. Not all potential glide planes are equivalent and they are likely to exhibit contrasting intrinsic resistance to plastic shear. Using ab initio methods, it is possible to calculate the ideal shear strength and to emphasize the anisotropic character induced by the complex chemistry. This approach is applied here to forsterite for the first time.

SLIP SYSTEMS IN OLIVINE

Geologically relevant olivines belong to a solid-solution between two end-member phases: forsterite (Fo) Mg_2SiO_4 and fayalite (Fa) Fe_2SiO_4. Olivines from the upper mantle have a Mg-rich composition (ca. Fo90). The present study will focus on forsterite alone. The structure of olivine is based on a distorted hexagonal close-packed oxygen sublattice. The Bravais lattice is orthorhombic (space group *Pbnm*) with *b* being almost twice as long as *a* and *c* (see Table 1). The unit cell contains four formula units.

Numerous deformation experiments have been performed on olivine and forsterite single crystals (Kohlstedt and Goetze 1974; Durham 1975; Durham and Goetze 1977; Durham et al. 1977, 1979; Darot and Gueguen 1981; Gueguen and Darot 1982) with a view to characterizing the slip systems. In most cases, experiments have been performed along the pseudo-cubic orientations $[101]_c$, $[110]_c$, and $[011]_c$ which allow activation of

* E-mail: patrick.cordier@univ-lille1.fr

0003-004X/05/0007–1072$05.00/DOI: 10.2138/am.2005.1738

single or duplex slips. The most common dislocations observed have Burgers vectors **b** that correspond to the shortest lattice repeats: [100] and [001]. [010] dislocations, scarcely observed, do not seem to participate in plastic deformation of olivine. Since the lattice parameter *b* is large in this structure, the absence of [010] dislocations is usually interpreted on energetic grounds (the elastic energy of [010] dislocations would be three to four times as large as for dislocations with [100] or [001] Burgers vectors). However, it is known that dislocations with Burgers vectors of the same order of magnitude exist in wadsleyite, which is a high-pressure polymorph of olivine (Thurel et al. 2003), but they are dissociated. The easiest slip systems at high temperature (i.e., above ca. 1000 °C) involve [100] slip on several planes: (010), {031}, {021}, {011}, and (001). Cross slip between these different planes is frequent. At low temperature and/or high strain-rate, slip occurs along [001] in (100), {110}, and (010).

COMPUTATIONAL METHODS

The calculations were performed using the ab initio total-energy calculation package VASP (Vienna Ab initio Simulation Program) developed at the Institut für Materialphysik of the Universität Wien (Kresse and Hafner 1993; Kresse and Furthmüller 1996a,b). This code is based on the first-principles density functional theory and solves the effective one-electron Hamiltonian involving a functional of the electron density to describe the exchange-correlation potential. It gives access to the total energy of a periodic system with no experimental input except the atomic number of the atoms. Computational efficiency is achieved using a plane-wave basis set for the expansion of the single electron wave functions and fast numerical algorithms to perform self-consistent calculations. All the calculations presented here were made with the Generalized Gradient Approximation (GGA) derived by Perdew and Wang (1992). Ultrasoft pseudopotentials (Vanderbilt 1990; Kresse and Hafner 1994a, 1994b) were used for Mg, Si, and O with an outmost core radius of 1.058, 0.953, and 0.820 Å, respectively. $2p^6$ and $3s^2$ were considered as valence electrons for Mg, whereas for Si and O the valence electrons were $3s^2\,3p^2$ and $3s^2\,3p^4$, respectively. Convergence tests for the lattice parameters and the total energy of the olivine showed that energy values converging to better than 0.5 meV/atom were obtained for a plane-wave cut-off of 600 eV, a value thus used throughout this work. The values of the calculated lattice parameters are reported Table 1.

The first Brillouin zone was sampled using a Monkhorst-Pack grid (Monkhorst and Pack 1976). For the forsterite orthorhombic unit-cell, using a $3 \times 2 \times 3$ mesh leads to convergence of the energy within the range defined above. When using other types of supercells, the *k*-points grid was chosen to keep as constant as possible the *k*-points density in reciprocal space. Using similar parameters in the local density approximation, Kiefer et al. (2001) obtained a good description of wadsleyite, a high-pressure polymorph of the silicate studied here.

To calculate the nine elastic constants of the orthorhombic forsterite, we strained the equilibrium cell using adapted deformations. In the strained configuration, the atoms were allowed to relax, the relaxation being completed when the magnitude of the forces on the atoms was lower than 0.02 eV/Å. The magnitude of the applied strain was lower than 2% and negative and positive values were used. The elastic constants presented in Table 2 were obtained from the fit of the total energy vs. strain by second-order polynomials. The standard deviation of the second-order coefficient allows the error on the calculated elastic parameters to be estimated to be less than 2% (except for C_{44}, for which the error is less than 3.5%).

The calculation of the generalized stacking-fault (GSF) excess energies was done in the following way. First, a stacking plane was chosen; here we present results concerning the (100), (010), (001), (110), and (021) planes. For a given stacking plane, two lattice translations in the plane, perpendicular to each other, were chosen as principal directions for the supercell used to model the GSF; their magnitudes a_s and b_s are reported in Table 3. The third supercell direction $[001]_s$ was chosen perpendicular to the GSF plane. Since forsterite does not have cubic symmetry, $[001]_s$ is not in general a lattice translation, which implies that when periodic lattice conditions are applied, the upper and lower part of the supercell do not necessarily fit together. To avoid this difficulty and to calculate GSF excess energies for any fault vector **u** (see below), a vacuum buffer 6 Å thick was added to the stacking of atomic planes along $[001]_s$. We verified that neither increasing the thickness of the vacuum buffer nor the addition of substance parallel to the stacking-fault plane significantly modifies the GSF excess energies. Therefore, in spite of long-range interactions, the slabs of material used in this work are thick enough to satisfactory reproduce energy differences between faulted and non-faulted configurations. Other supercell symmetries can be used but the choice of an orthorhombic one with $[001]_s$ direction perpendicular to the fault plane facilitates atomic relaxations that will be performed in a subsequent work.

The number and the types of atoms included in each supercell are reported in Table 3, while a schematic of a typical supercell used to calculate (021) GSF is given in Figure 1. Once the supercell was built, the upper part of the supercell was moved with respect to the lower one by **u**, the fault vector contained in the fault plane and the magnitude of which can be adjusted. In most cases, the fault plane was chosen to preserve the SiO_4 structural tetrahedron as shown in Figure 1. Once the translation was made, the atoms were not allowed to relax. As a consequence, the GSF values presented here are an upper bound for the relaxed values.

RESULTS AND DISCUSSION

Energy barriers associated with plastic shear

Our calculations provide us with the energy barrier associated with a rigid shear along the most common slip systems in forsterite. In minerals, plastic shear usually occurs along cationic layers (i.e., corrugated surfaces) between the SiO_4 tetrahedra. For olivine, which has a compact structure and exhibits an almost close-packed oxygen sublattice, such a glide may imply a considerable impingement for some of the atoms. If the impingements and the proportion of involved atoms are large, a high energy barrier, and hence a considerable lattice friction (leading to a very large flow stress) will result. Figure 2 shows that the easiness of shear along [100] seems to be very comparable with (010) and (001) and easier along (021). In any case, the energy barriers are symmetrical and exhibit almost the same maxima, only the shapes are slightly different. It is usually considered that SiO_4 tetrahedra are strong units in silicates. We have thus taken care in the above calculations to choose the cutting level between the

TABLE 1. Crystallographic data for forsterite at room *P* and *T* compared with calculated data

	a (Å)	*b* (Å)	*c* (Å)	*V*(Å³)	Density (Mg/m³)
Experimental (Fujino et al. 1981)	4.7534	10.1902	5.9783	289.58	3.227
Calculated LDA (Wentzcovitch and Stixrude 1997)	4.682	9.953	5.837	272	3.436
Calculated LDA (Brodholt et al. 1996)	4.643	9.988	6.074	281.67	3.318
Calculated GGA (Brodholt 1997)	4.71	10.15	5.96	284.92	3.280
Calculated GGA (this study)	4.793	10.281	6.041	297.68	3.139

TABLE 2. Elastic constants for forsterite at room *P* and *T* compared with calculated data

	C_{11} (GPa)	C_{22} (GPa)	C_{33} (GPa)	C_{44} (GPa)	C_{55} (GPa)	C_{66} (GPa)	C_{12} (GPa)	C_{13} (GPa)	C_{23} (GPa)
Experimental (Graham and Barsch 1969)	329.1	200.5	236.3	67.2	81.4	81.4	66.3	68.4	72.8
Experimental (Kumazawa and Anderson 1969)	328.4	199.8	235.3	65.9	81.2	80.9	63.9	68.8	73.8
Experimental (Hearmon 1979)	328	200	235	66.7	81.3	80.9	69	69	73
Calculated LDA (da Silva et al. 1997)	367	220	233	78.4	88.7	90.8	77.8	79.3	80.6
Calculated (this study)	300.7	195.7	224.1	65.8	78.3	77.3	61.1	62.2	64.7

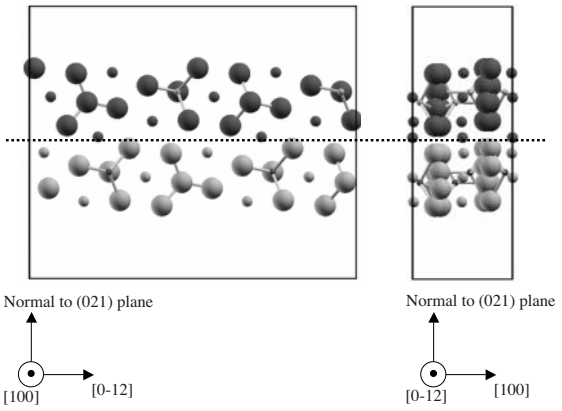

FIGURE 1. Unsheared supercell used to calculate (021) stacking fault. The upper part of the supercell (where O and Mg ions are represented as dark balls and Si ions, in the center of the tetrahedron, are represented as small light balls) is moved with respect to the lower one (where O and Mg ions are represented as light balls and Si ions, in the center of the tetrahedron, are represented as small dark balls). In this case, the fault vector **u** is along [100] and the fault plane does not break Si-O bonds

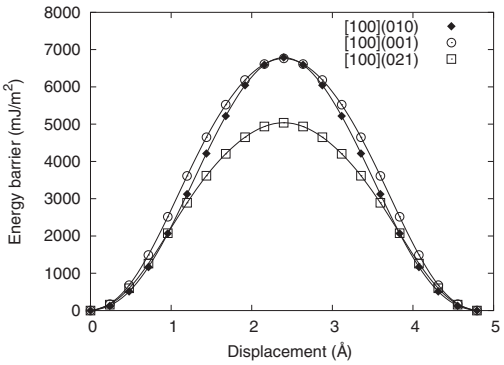

FIGURE 2. Generalized stacking fault energy as a function of displacement along [100] on (010), (001), and (021).

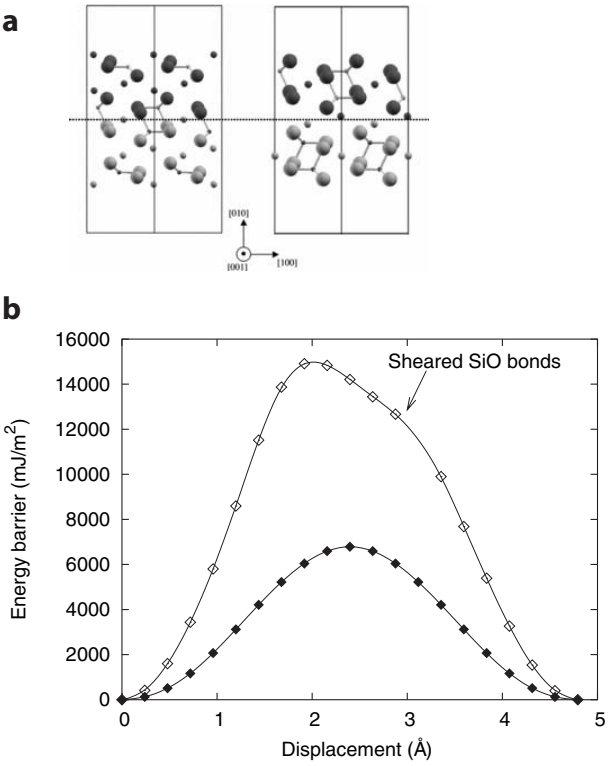

FIGURE 3. (**a**) Unsheared supercells (two are represented along the [100] direction) used to calculate the generalized stacking fault on (010) with the fault vector **u** along [100]. For the left one, the fault plane (represented by the dotted line) cuts the Si-O bonds, whereas the right one does not. (**b**) Generalized stacking fault energy as a function of displacement along [100] on (010) corresponding to the two cutting levels represented in Figure 3a.

TABLE 3. Characteristics of the supercells used for calculating the GSF; a_s, b_s, and c_s represent the lattice parameters of the supercells

Direction of the fault or slip vector **u**	Stacking fault plane	a_s (Å)	b_s (Å)	c_s (Å)	*k*-points grid	Atoms in the supercell
[100]	(001)	4.793	10.281	12.04	3 × 2 × 1	8Mg, 4Si, 16O
	(010)	4.793	6.041	16.281	3 × 3 × 1	8Mg, 4Si, 16O
	(021)	4.793	15.864	13.3	3 × 1 × 1	16Mg, 8Si, 32O
[001]	(100)	6.041	10.281	10.793	3 × 2 × 2	8Mg, 4Si, 16O
	(010)	4.793	6.041	16.281	3 × 3 × 1	8Mg, 4Si, 16O
	(110)	6.041	11.343	14.6	3 × 2 × 1	16Mg, 8Si, 32O

SiO_4 layers (see Fig. 1). This condition can be fulfilled in most cases in olivine, which is composed of isolated SiO_4 tetrahedra. To evaluate the cohesive character of the SiO_4 tetrahedra, we performed one calculation on the [100](010) slip system with a cut through the Si-O bonds (Fig. 3a). Figure 3b shows that the energy barrier associated with this cut is much greater than the one previously calculated. This confirms the hypothesis that shear in silicates tends to be localized in planes which do not cut the strong Si-O bonds. (100), {110}, and (010) are such planes for [001] slip. Figure 4 shows that the energy barrier associated with [001] slip in (010) is the lowest, making this slip system the easiest intrinsically. This is in agreement with the fact that [001] shear is easier at low temperature. The case of the [001](100) and [001]{110} barriers (with their "camel-hump" shapes) is interesting because they exhibit an intermediate minimum suggesting the possibility of a stable stacking fault in the (100) and {110} planes along [001]. Finally, we tested the possibility of achieving plastic shear along the [010] direction in (100) and (001). Figure 5 shows that shear along [010] in (001) is associated with an energy barrier which is higher than the one corresponding to plastic shear along [100] across the Si-O bonds. The possible existence of a stable stacking fault is suggested however in this system. The situation is more unfavorable in the case of shear along [010] in (100) (Fig. 5), which brings SiO_4 tetrahedra very close to the oxygen atoms.

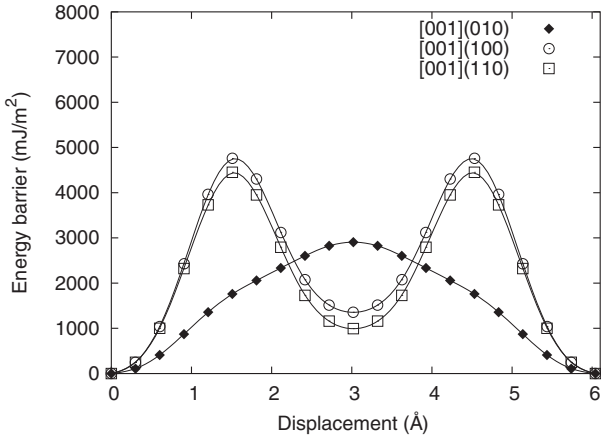

FIGURE 4. Generalized stacking fault energy as a function of displacement along [001] on (010), (100), and (110).

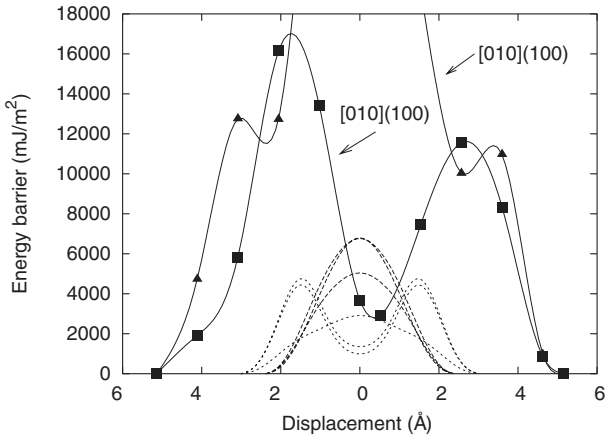

FIGURE 5. Generalized stacking fault energy as a function of displacement along [010] on (100) and (001). GSF energies corresponding to [100] and [001] glides are superimposed for comparison. Note that relative displacements **u** associated with [100], [010], and [001] glides correspond physically to different lengths.

Ideal shear strength

From the energy profiles depicted in Figures 2 to 4, an upper bound on the yield strength can be established by considering the ideal (theoretical) shear strength of the perfect crystal. Although these values are rarely reached in practice, the concept of ISS has proved to be of major interest in the theory of plastic deformation. The calculation of the ideal shear strength is new in the context of mineral physics. However, it has received increasing attention in recent years, mostly with respect to metals: Al (Paxton et al. 1991; Sun and Kaxiras 1997; Hartford et al. 1998; Ogata et al. 2002), Cu (Paxton et al. 1991; Ogata et al. 2002), Mo (Xu and Moriarty 1996), Pd (Hartford et al. 1998), Ta (Söderlind and Moriarty 1998), NiAl and FeAl (Medvedeva et al. 1996). Other materials (oxides, ceramics, semiconductors) have only rarely been considered [see Kocer et al. (2003) for cubic silicon nitride]. Paxton et al. (1991) define the theoretical or ideal shear strength as the "maximum resolved shear stress that an ideal, perfect crystal can suffer without plastically deforming". The ideal shear strength can be calculated from the finite-strain elastic instability of a perfect lattice undergoing homogeneous deformation (Roundy et al. 1999; Yip et al. 2001; Kocer et al. 2003) or alternatively from the restoring force $\overline{F} = -\text{grad}\gamma(\overline{u})$ in the generalized stacking fault picture (Vítek 1974; Medvedeva et al. 1996; Sun and Kaxiras 1997; Hartford et al. 1998). Note that both methods, being path-dependent, do not necessarily give the same results. We have used the latter approach to calculate the maximum stress, τ_{max}, that gives a qualitative estimation of the shear resistance. Figure 6 shows an example of such a calculation for the [100](010) slip system. The ideal shear strength is identified with the maximum of the calculated stress τ_{max} along the shear displacement. The results of the calculations are presented in Table 4. As expected from the energy barriers, [001](010) appears to be the intrinsically easiest slip system in olivine. The calculated $\tau_{max} = 0.24\mu$ (μ is the shear modulus) is close to the Frenkel behavior which corresponds to a sine function for the energy barrier (Frenkel 1926). The other slip systems exhibit higher values of τ_{max} in the range 0.42–0.66μ. For comparison, most metals yield values in the range 0.09–0.17μ (Paxton et al. 1991; Söderlind et al. 1998; Roundy et al. 1999; Krenn et al. 2001).

Implications on dislocations and plasticity of forsterite

Relying on the concept of ISS, our results provide the first physical basis to account for plastic shear anisotropy in forsterite. We have shown that the [010] glide is inhibited not only by the high level of the elastic energy, but also by the difficulty

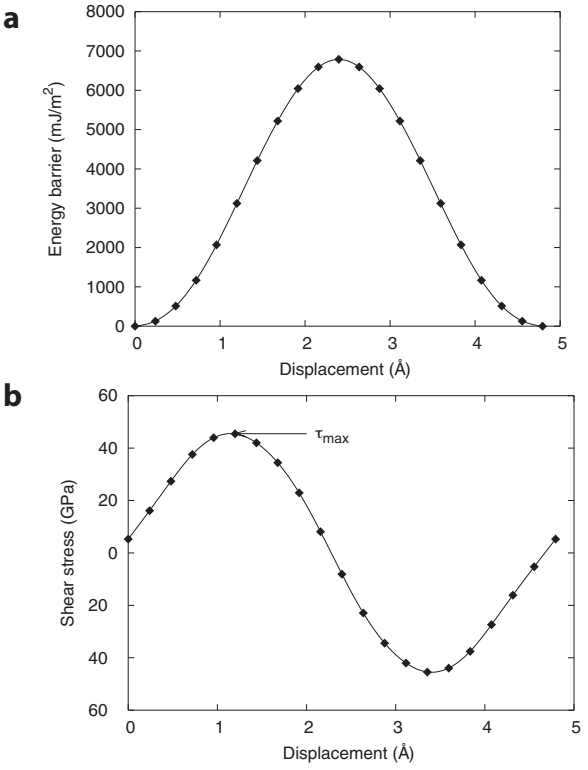

FIGURE 6. Calculated ideal shear stress for [100](010). The energy barrier is shown in the upper panel (**a**) whereas the shear stress (derivative of the energy barrier) is shown in the lower panel (**b**). The ideal shear stress is identified with the maximum stress.

TABLE 4. Calculated values of the ISS (τ_{max}); for comparison, the ISS are normalized by the anisotropic shear moduli $\mu_{[uvw](hkl)}$ calculated for each slip system and presented on the first line

	[100](001)	[100](010)	[100](021)	[001](100)	[001](010)	[001](110)
$\mu_{[uvw](hkl)}$ (GPa)	81.3	80.9	81.1	81.3	66.7	68.9
τ_{max} (GPa)	45.8	45.5	34	50.8	16.1	45.2
τ_{max} / $\mu_{[uvw](hkl)}$	0.56	0.56	0.42	0.62	0.24	0.66

Note: For more details on the calculation of anisotropic shear moduli, see Thurel et al. (2003).

of achieving plastic shear along this direction. It must be noted however that the energy barrier associated with plastic shear in the system [010](001) suggest the possibility of a stable stacking fault and hence of dissociated dislocation within this plane. In contrast, the [100] glide is associated with a smooth energy barrier which is very close to a sinusoidal potential on (010) and (001). Our calculations suggest that the [100] glide would be intrinsically more easy on (021) which exhibits a lower τ_{max}. It is thus expected that this slip system should have the lower critical resolved shear stress (among [100] glide systems), at least at low temperature. However, to the best of our knowledge there is no single-crystal data to check this point. Finally, our calculations shed new light on the [001] glide in olivine. We have shown that the glide system which exhibits the lowest intrinsic resistance to plastic shear in olivine is [001](010), in agreement with existing experimental data at low temperature. In this system, the energy barrier is smooth and exhibits no intermediate minimum. Two slip systems exhibit energy barriers with a marked camel-hump suggesting a possible stacking fault in the three planes (100), (110), and $(1\bar{1}0)$.

Further calculations incorporating ionic relaxations are necessary to assess quantitatively the stacking fault energy and the possibility for dislocation dissociation. Moreover, such data should allow estimation of the Peierls-Nabarro stress τ_{PN} (Christian and Vitek 1970) which can be more easily linked to low-temperature experimental data. At the present time our calculations give a first hint for understanding the marked anisotropy for [001] dislocation mobility. [001] straight screw dislocations suggest strong lattice friction. In analogy with the bcc case, [001] dislocation cores might be non-planar with spreading in the three (100), (110), and $(1\bar{1}0)$ planes.

First-principles calculations of ideal shear strengths provide a rational picture for the anisotropy of plastic shear of forsterite in connection with the crystal chemistry. From the present study, the various slip systems can be sorted as: easy = [001] glide, especially on (010); intermediate = [100] glide [with (021) appearing as the easiest plane]; difficult = [010] glide.

This is consistent with the low-temperature plasticity of forsterite. The present work clearly shows that the ideal shear strength concept is, in spite of its simplicity, extremely relevant to decipher the influence of the crystal chemistry on plastic shear. From this point of view, this fundamental approach improves the understanding of mechanical properties of minerals and must be seen as the groundwork for further more sophisticated calculations.

ACKNOWLEDGMENTS

This work was supported by CNRS-INSU under the DyETI program. Computational resources were provided by IDRIS (project no. 031685) and CRI-USTL, which are supported by the Fonds Européens de Développement Régional.

REFERENCES CITED

Brodholt, J. (1997) Ab initio calculations on point defects in forsterite (Mg_2SiO_4) and implications for diffusion and creep. American Mineralogist, 82, 1049–1053.

Brodholt, J., Patel, A., and Refson, K. (1996) An ab initio study of the compressional behavior of forsterite. American Mineralogist, 81, 257–260.

Christian, J.W. and Vítek, V. (1970) Dislocations and stacking faults. Reports on Progress in Physics, 33, 307–411.

Darot, M. and Gueguen, Y. (1981) High-temperature creep of forsterite single crystals. Journal of Geophysical Research, 86(B7), 6219–6234.

da Silva, C., Stixrude, L., and Wentzcovitch, R.M. (1997) Elastic constants and anisotropy of forsterite at high pressure. Geophysical Research Letters, 24, 1963–1966.

Durham, W.B. (1975) Plastic flow of single crystals of olivine. Ph.D. thesis, M.I.T., Cambridge.

Durham, W.B. and Goetze, C. (1977) Plastic flow of oriented single crystals of olivine. 1. Mechanical Data. Journal of Geophysical Research, 82, 5737–5753.

Durham, W.B., Goetze, C., and Blake, B. (1977) Plastic flow of oriented single crystals of olivine. 2. Observations and interpretations of the dislocation structures. Journal of Geophysical Research, 82, 5755–5770.

Durham, W.B., Froidevaux, C., and Jaoul, O. (1979) Transient and steady-state creep of pure forserite at low stress. Physics of the Earth and Planetary Interiors, 19, 263–273.

Frenkel, J. (1926) Zur Theorie der Elastizitätsgrenze und der Festigkeit kristallinischer Körper, 37, 572.

Fujino, K., Sasaki, S., Takeuchi, Y., and Sadanaga, R. (1981) X-ray determination of electron distributions in forsterite, fayalite, and tephroite. Acta Crystallographica, B37, 513–518.

Graham, E.K. and Barsch, G.R. (1969) Elastic constants of single crystals forsterite as a function of temperature and pressure. Journal of Geophysical Research, 74, 5949–5960.

Gueguen, Y. and Darot, M. (1982) Les dislocations dans la forsterite déformée à haute température. Philosophical Magazine A, 45, 419–442.

Hartford, J., von Sydow, B., Wahnström, G., and Lundqvist, B.I. (1998) Peierls barrier and stresses for edge dislocations in Pd and Al calculated from first principles. Physical Review B, 58, 2487–2496.

Hearmon, R.F.S. (1979) The elastic constants of crystals and other anisotropic materials. In K.H. Hellwege and A.M. Hellwege, Eds., Landolt-Börnstein Tables, III, p. 1–244. Springer Verlag, Berlin.

Kiefer, B., Stixrude, L., Hafner, J., and Kresse, G. (2001) Structure and elasticity of wadsleyite at high pressures. Americal Mineralogist, 86, 1387–1395.

Kocer, C., Hirosaki, N., and Ogata, S. (2003) Ab initio calculation of the ideal tensile and shear strength of cubic silicon nitride. Physical Review B, 67, 035210–035214.

Kohlstedt, D.L. and Goetze, C. (1974) Low-stress high-temperature creep in olivine single crystals. Journal of Geophysical Research, 79, 2045–2051.

Krenn, C.R., Roundy, D., Morris Jr., J.W., and Cohen, M.L. (2001) The nonlinear elastic behavior and ideal shear strength of Al and Cu. Materials Science Engineering A, 317, 44–48.

Kresse, G. and Furthmüller, J. (1996a) Efficiency of ab-initio total energy calculations for metals and semiconductors using a plane-wave basis set. Computational Materials Science, 6, 15–50.

——— (1996b) Efficient iterative schemes for ab initio total-energy calculations using a plane-wave basis set. Physical Review B, 54, 11169.

Kresse, G. and Hafner, J. (1993) Ab initio molecular dynamics for liquid metals. Physical Review B, 47, 558.

——— (1994a) Ab initio molecular dynamics simulation of the liquid-metal amorphous-semiconductor transition in germanium. Physical Review B, 49, 14251.

——— (1994b) Norm-conserving and ultrasoft pseudopotentials for first-row and transition elements. Journal of Physics Condensed Matter, 6, 8245.

Kumazawa, M. and Anderson, O.L. (1969) Elastic moduli, pressure derivatives and temperature derivatives of single crystal olivine and single crystal forsterite. Journal of Geophysical Research, 74, 5961–5972.

Medvedeva, N.I., Mryasov, O.N., Gornostyrev, Y.N., Novikov, D.L., and Freeman, A.J. (1996) First-principles total-energy calculations for planar shear and cleavage decohesion processes in B2-ordered NiAl and FeAl. Physical Review B, 54, 13506–13514.

Monkhorst, H.J. and Pack, J.D. (1976) Special points for Brillouin-zone integrations. Physical Review B, 23, 5048–5192.

Ogata, S., Li, J., and Yip, S. (2002) Ideal pure shear strength of aluminum and copper. Science, 298, 807–811.

Paxton, A.T., Gumbsch, P., and Methfessel, M. (1991) A quantum mechanical calculation of the theoretical strength of metals. Philosophical Magazine Letters, 63, 267–274.
Perdew, J.P. and Wang, Y. (1992) Accurate and simple analytic representation of the electron-gas correlation energy. Physical Review B, 45, 13244–13249.
Rasmussen, T., Jacobsen, K.W., Leffers, T., and Pedersen, O.B. (1997) Simulations of the atomic structure, energetics, and cross slip of screw dislocations in copper. Physical Review B Condensed Matter, 56(6), 2977–2990.
Roundy, D., Krenn, C.R., Cohen, M.L., and Morris Jr., J.W. (1999) Ideal shear strengths of fcc aluminum and copper. Physical Review Letters, 82, 2713–2716.
Söderlind, P. and Moriarty, J.A. (1998) First-principles theory of Ta up to 10 Mbar pressure: Structural and mechanical properties. Physical Review B, 57, 10340–10350.
Sun, Y. and Kaxiras, E. (1997) Slip energy barrier in aluminum and implications for ductile-brittle behaviour. Philosophical Magazine A, 75, 1117–1127.
Thurel, E., Douin, J., and Cordier, P. (2003) Plastic deformation of wadsleyite: III. Interpretation of dislocations and slip systems. Physics and Chemistry of Minerals, 30, 271–279.
Vanderbilt, D. (1990) Soft self-consistent pseudopotentials in a generalized eigenvalue formalism. Physical Review B, 41, 7892–7895.
Vítek, V. (1974) Theory of the core structures of dislocations in body-centered-cubic metals. Crystal Lattice Defects, 5, 1–34.
Wentzcovitch, R.M. and Stixrude, L. (1997) Crystal chemistry of forsterite: a first-principles study. American Mineralogist, 82, 663–671.
Xu, W. and Moriarty, J.A. (1996) Atomistic simulation of ideal shear strength, point defects, and screw dislocations in bcc transition metals: Mo as a prototype. Physical Review B, 54, 6941–6951.
Yip, S., Li, J., Tang, M., and Wang, J. (2001) Mechanistic aspects and atomic-level consequences of elastic instabilities in homogeneous crystals. Materials Science Engineering, A317, 236–240.

MANUSCRIPT RECEIVED JUNE 3, 2004
MANUSCRIPT ACCEPTED NOVEMBER 9, 2004
MANUSCRIPT HANDLED BY KARSTEN KNORR